Nano Energy (2012) 1, 534–551

Available online at www.sciencedirect.com

SciVerse ScienceDirect

journal homepage: www.elsevier.com/locate/nanoenergy

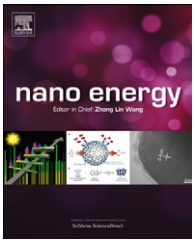

REVIEW

Graphene for energy conversion and storage in fuel cells and supercapacitors

Hyun-Jung Choi[a], Sun-Min Jung[a], Jeong-Min Seo[a], Dong Wook Chang[b], Liming Dai[c], Jong-Beom Baek[a,*]

[a]*Interdisciplinary School of Green Energy/Low-Dimensional Carbon Materials Center, Ulsan National Institute of Science and Technology (UNIST), 100 Banyeon, Ulsan 689-798, South Korea*
[b]*Department of Chemical Systematic Engineering, Catholic University of Daegu, 13-13 Hayang, Gyeongbuk 712-702, South Korea*
[c]*Department of Macromolecular Science and Engineering, Case Western Reserve University, 10900 Euclid Avenue, Cleveland, OH 44106, USA*

Received 19 March 2012; received in revised form 1 May 2012; accepted 1 May 2012
Available online 15 May 2012

KEYWORDS
Graphene;
Energy conversion;
Energy storage;
Fuel cell;
Supercapacitor

Abstract
Due to its high specific surface area, good chemical stability and outstanding electrical properties, graphene, a class of two-dimensional allotrope of carbon-based materials, is one of ideal candidates for next generation energy conversion and storage devices. In this review, we will present an overview on electrochemical characteristics of graphene by summarizing the recent research trend on graphene for energy conversion and storage applications, such as fuel cells and supercapacitors, along with some discussions on future research directions.

Introduction

Due to the rapid industrial development and growing human population, along with the increase in energy demand, the global energy consumption has been accelerating at an alarming rate. At current consumption rate, global energy exhaustion will become inevitable. To prevent disaster caused by energy exhaustion, the need for renewable energy sources has attracted tremendous attention around the world. In order to make the effective use of renewable energy, it is important to develop high-performance, low-cost and environmental-friendly energy conversion and storage systems. Fuel cells and supercapacitors are the systems required for promising electrochemical energy conversion and storage. Fundamentally, the performance of those systems is directly related to the material properties. Therefore, material technology plays a pivotal role in the development of electrochemical energy conversion and storage systems. Among the various materials, which have been investigated in these electrochemical devices, carbon materials are of great interest owing to their abundance, stability and relative environmental-friendliness. In particular, the excellent chemical stability across a wide

*Corresponding author. Tel.: +82 52 217 2510; fax: +82 52 217 2019.
E-mail address: jbbaek@unist.ac.kr (J.-B. Baek).

2211-2855/$ - see front matter © 2012 Elsevier Ltd. All rights reserved.
http://dx.doi.org/10.1016/j.nanoen.2012.05.001

temperature range in either acidic or basic media makes carbon materials extremely attractive for use as electrodes in electrochemical energy devices [1].

There are many available carbon allotropes, such as buckyminsterfullerene, carbon nanotube, graphene and nanodiamond. Among them, graphene, a single layer of two-dimensional honeycomb carbon lattice, is one of the carbon family discovered a few years ago [2] and is emerged as exciting novel material. Graphene has unique properties, including high specific surface area (2630 m^2/g) [3], good chemical stability and excellent electrical conductivity. These properties make graphene to be an excellent candidate for energy conversion and storage applications.

This review will focus on graphene as a material for energy conversion and storage applications. We will first give a brief overview on graphene. This will then be followed by discussions on the electrochemical applications of graphene in energy conversion and storage devices, including fuel cells and supercapacitors.

Graphene: overview

Graphene as one of the carbon allotropes was experimentally discovered in 2004 for the first time [2], which consists of a flat monolayer of sp^2 bonded carbon atoms into a two-dimensional (2D) honeycomb lattice. It is the basic building block of all the ''graphitic'' materials such as fullerene (0D), carbon nanotube (1D) and graphite (3D) [4]. In fact, two-dimensional crystals like graphene was predicted theoretically to not exist because strictly 2D crystals were thought to be thermodynamically unstable at finite temperature [4]. However, in 2004, Geim and co-workers at Manchester University first isolated single-layer, two-dimensional crystal from graphite by using peel-off method, so called, Scotch-tape method [2]. This led to an explosion of interest, and much research has been conducted on the structure and property characterization of graphene. Table 1 lists some unusual properties of graphene compared with other carbon materials.

These remarkable properties enable us to make graphene useful for device applications. For example, graphene has been made into semiconductors in the form of nanoribbons (GNRs), leading to graphene field-effect transistors (FETs) [23]. Also, graphene powder is considered to be excellent filler for composite materials [24]. Moreover, transparent graphene thin films are often suggested as a competitor for indium tin oxide (ITO). Therefore, it can be used as transparent electrodes [25] in solar cells [26] and light-emitting diodes [27]. Furthermore, graphene has emerged as a viable candidate for use in optoelectronics [28] and sensors [29]. Of course, there is fast-growing interest in the electrochemical applications using graphene and graphene-based materials, as we will discuss in this review.

Since graphene was discovered by mechanical exfoliation using Scotch-tape in 2004, many routes have been introduced to achieve a high-quality and large-area graphene. Information about how the graphene was prepared is important, because the properties of graphene strongly depend on preparation methods. The reported methods are generally fit into two major approaches that are ''top-down'' and ''bottom-up'' approaches. The meaning of top-down approach implies

Table 1 Properties of carbon materials.

Properties	Fullerenes	Carbon nanotubes	Activated carbon	Graphite	Graphene
Specific surface area (m^2/g)	5 [5]	1315 [3]	1200 [6]	~10 [1]	2630 [3]
Thermal conductivity (W/m K)	0.4 [7]	>3000 (multi-walled carbon nanotube) [8]	0.15-0.5 [9]	~3000 (in-plane values) [10]	~5000 [11]
Intrinsic mobility (cm^2/V s)	0.56 [12]	~100,000 [13]	-	13,000 (in-plane values) [14]	~15,000 (in-plane values onto SiO_2 surface) ~200,000 (free-standing) [15,16]
Young's modulus (TPa)	0.01 [17]	0.64 [18]	0.138 [19]	1.06 [20]	~1.0 [21]
Optical transparency (%)	-	-	-	-	~97.7 [22]

the exfoliation of natural or synthetic graphite into the mixture of a single and a few layer graphene platelets. Graphite into graphite oxide, which is precursor of graphene oxide (GO), is the most representative example of the top-down approach [30,31]. Also, liquid-phase exfoliation [32], graphite intercalation compounds (GICs) [33] and electrochemical exfoliation [30] are all included in top-down approaches. These approaches have the advantages for scalable and low-cost production. However, it is hard to obtain single-layer graphene with high-quality because of defect creation during exfoliation. In particular, reduction of GO into graphene results in a graphitic structure that is also one-atom thick, but it still contains large number of defects, such as nanoholes and Stone–Wales defect (heptagon/pentagon bonded carbon atom network) [34]. On the other hand, bottom-up approaches, which are directly growing graphene from organic precursors such as methane and other hydrocarbon sources [35], include epitaxial growth [36] and chemical vapor deposition (CVD) [37]. Bottom-up approach is one of the most attractive methods for high-quality and large-area graphene production [25]. Particularly, CVD grown graphene has been demonstrated to be of promise for potential applications as transparent electrodes [25]. However, bottom-up approaches are extremely difficult to control manufacturing process, and thus they result in high manufacturing cost.

Graphene: exciting properties for energy material

There is a reason why graphene is a good base material for energy conversion and storage applications; graphene has a good electrical conductivity and high surface area (see Table 1). Electrical conductivity is caused by its unique electronic properties, which include massless Dirac fermion, ambipolar electric field effect and extremely high carrier mobility [4]. These properties arise from the unique electronic structure of graphene. Intrinsically, graphene is a zero-gap conductor. Moreover, the charge carriers of graphene behave as massless Dirac fermions. As a result, the electrons in graphene lose their effective mass, which results in quasi-particles that are described by a Dirac-like equation rather than the Schrödinger equation with the Fermi velocity $\upsilon_F = 1 \times 10^6$ m/s [38]. In addition, the high quality of its 2D crystal lattice presents surprisingly fast transport properties. The high quality of graphene implies a low density of defects and graphene behaves like a metal with high constant mobility. In 2005, Novoselov and Geim at Manchester University measured carrier mobility to be 15,000 $cm^2/V\,s$ for a single layer of graphene onto silicon dioxide (SiO_2) layer, and the value were independent of temperature T between 10 and 100 K [15]. Furthermore, Kim's group at Columbia University measured carrier mobility to be excess of 200,000 $cm^2/V\,s$ for a suspended graphene [16]. These two experiments and other experimental studies have shown that the ballistic transport properties of graphene are extremely sensitive to its local environment, including the number of layers, edge structures, ripples, defects, doping, etc. [39]. For example, the mobility of synthetic graphene like GO and CVD grown graphene, which have approximately 200 and 2000 $cm^2/V\,s$, respectively [40], are much lower than that of mechanically exfoliated graphene. Another important point about charge transport in graphene is ambipolarity. In the field-effect configuration, ambipolarity implies that carriers can be tuned continuously between holes and electrons in concentrations up to 10^{13} cm^2 by supplying the requisite gate bias. Under negative gate bias, the Fermi level drops below the Dirac point, introducing a significant population of holes into the valence band. On the other hand, under positive gate bias, the Fermi level rises above the Dirac point, promoting a significant population of electrons into the conduction band [35].

The second reason is its high surface area. In 2000, Peigney et al. studied the theoretical calculation of specific surface area (SSA) of the carbon nanotubes (CNTs) [3]. The surface area of one hexagon and calculated the SSA by dividing the weight of two carbon atoms, which is 1315 m^2/g, corresponding to one side of hexagonal surface. In the case of graphene, the SSA should be considered as two sides of hexagonal surface. Therefore, the SSA of graphene is calculated to be 2630 m^2/g. Compared to the graphite ($\sim$10 m^2/g) [1] or CNT (1315 m^2/g), graphene has outstanding theoretical SSA.

However, the reported SSA values of graphene have been much lower than that of the theoretical value (2630 m^2/g). Although graphene is characterized to consist of a single layer by electron microscopy, the values are in the range of 1000 and 1800 m^2/g [41]. This is because of the assembling nature of graphene driven by the van der Waals interactions between neighboring sheets. Graphene suffers from agglomeration and restacking during utilization as an electrode material and results in a loss of effective surface area [42]. Furthermore, most of the graphene materials reported in literatures are not pristine single-layer graphene. Most of them have tremendous chemical and topological defects, such as oxygenated groups and structural imperfectness. Thus, some techniques were applied to increase the porosities and/or SSA of graphene by rapid expanding graphite oxide [43], stacking small graphene sheets into a porous structure [34] or activation of graphene [44]. For example, a microwave assisted exfoliation of GO followed by activation with KOH displayed increased SSA up to 3100 m^2/g [44].

Until now, it might have been considered as the SSA is increased, electrochemical characteristics of graphene are increased. However, the SSA is not directly proportional to the electrochemical characteristics for the following two reasons. First, the surface area is increased as porosity increased, whereas the volumetric conductivity is decreased to reduce the number of conductive pathways [45]. Second, all parts of surfaces are not electrochemically accessible, which means that electrochemically active surface is different from nitrogen adsorption surface. Therefore, controlling the pore size is more important factor than increasing the porosity [44].

Graphene: importance of defect

As aforementioned, graphene has a potential for commercialization of the various devices due to its outstanding properties. However, it has an inherent limitation for pristine single-layer graphene (mechanically exfoliated graphene) to fabricate devices, specifically electrochemical

devices. Of course, the properties of graphene from mechanical exfoliation are the best compared to the GO and other synthetic graphene materials. Nevertheless, most of the literatures report energy devices on the basis of GO and doped-graphene, because of their availability. The major advantages of the GO are its low-cost and scalability. Energy conversion and storage devices are required for large-scale production. GO is usually manufactured by breaking apart graphite into the sheets of oxidized graphene *via* acid intercalation, oxidation and subsequent physical agitation typically by sonication to yield GO nanosheets [35]. This approach is relatively simple and easy for mass production compared with CVD. In addition, graphite, which is starting material for GO, is sold at a very low price at about a few cents per gram [41]. However, GO, the most widely used graphene-related material, suffers from its poor properties, such as low surface area, high-density of oxygenated functional groups and low electrical conductivity (insulator). Nevertheless, the presence of oxygen-containing groups at its surface or edges, sometimes, is advantageous to significantly influence the interfacial activity between graphene electrode and electrolyte. The oxygen-containing groups, such as epoxy and hydroxyl groups at basal plane and carbonyl and carboxylic groups at edges, can act as anchoring points for the attachment of other materials, such as polymers [46], metal oxides [42] and platinum (Pt) [47]. The polar nature of GO could also contribute to improved dispersion of composite materials on graphene sheets by preventing the aggregation [1]. Thus, these composites have been demonstrated a great electrochemical performance compared with GO itself and reduced GO (rGO) [48]. Moreover, oxygen-containing groups of the graphene may serve as active sites that can increase the density of oxygen at the electrode interface, which can catalyze the oxygen reduction reaction (ORR) [49]. On the other hand, the presence of surface oxygenated groups affects the resistivity of graphene [45]. For example, heteroatom like oxygen can reduce the electron or hole mobility and increase the resistivity. Therefore, it is important to control the density of oxygen-containing groups at GO for maximum performance.

Fuel cells

Carbon nanotubes (CNTs) have been investigated as catalyst supporting materials in fuel cell applications, which have shown enhanced catalytic activities [50,51]. However, many researchers have started to shift their research target towards graphene in the last few years after the existence of 2D graphene is reported [2,31,37,52]. Compared with CNTs, graphene has higher surface area and similar conductivity for electrochemical applications, but it can be produced at a much lower cost. Due to its outstanding properties as mentioned earlier, graphene has many potential applications. Amongst them, fuel cell draws tremendous attention as the upcoming alternative energy source. Because fuel cells are eco-friendly process to produce electricity, water and heat only with no pollutant or toxic by-product, many researches are now focusing on cost down and efficiency up fuel cells. Fuel cells consist of three key parts: cathode, anode and separation membrane. Among them, cathode materials are pivotal elements for the commercialization. Currently, expensive noble metals such as platinum (Pt), gold (Au), ruthenium (Ru), and their alloys are best known cathode materials for oxygen reduction reaction (ORR) [42,53–56]. Among them, Pt is the most widely studied noble metal as electrocatalyst. However, it is too expensive and limited reserve in earth. Thus, there must be at least one of three ways to solve the issues. One is to minimize the use of expensive catalysts by increasing surface area *via* nanoparticle approach [57,58]. Another is to find alternative cheap but efficient metal catalysts to replace expensive noble metals [59,60]. The last is to develop efficient metal-free catalysts. Although Pt-based catalysts have been widely studied and commercialized due to their high current density and low over-potential [45,55,61,62], there are still intensive efforts required for further maximizing the activity of Pt and minimize the use of Pt. It is very necessary to load nanostructured Pt with high activity on the surface of supporting nanomaterials with low cost, high surface area and good electrical conductivity. In this way, not only the availability of nanosized electrocatalyst surface area can be maximized for efficient electron transfer, but also the mass transport of reactants to the electrocatalyst can be provided more effectively [47,55,62]. Nevertheless, Pt-based catalysts still suffer from poor tolerance against carbon monoxide poisoning and fuel crossover. Thus, the development of a new class of materials with low-cost, high-efficiency for ORR and good durability is required to boom fuel cells as one of the most promising energy sources. In this regard, carbon based metal-free electrocatalysts are developed with high catalytic activity, long cycle stability, low poisoning effect and anode crossover [51,59]. However, there are still remaining challenges to develop metal-free ORR catalysts with a further decreasing over-potential comparable to Pt, high current density and durability in acidic media. In this section, these aspects in fuel cell will be overviewed.

Pt/graphene hybrids

To enhance the ORR electrocatalytic activity, Honma and co-workers [62] have investigated that Pt nanoparticles supported on graphene nanosheet (GNS), which were prepared by using $Pt(NO_2)_2 \cdot NH_3)_2$ as Pt precursor and GNS powder, followed by annealing in Ar/H_2 (4:1 v/v) at 400 °C for 2 h. The loading amount (about 20 wt%) of Pt clusters to GNS is determined by inductively coupled plasma (ICP) analysis and the amount is approximately similar to Pt on activated carbon (Pt/C, Vulcan XC-72R) for fair comparison. In this particular case, there are two types of Pt clusters have been observed with high-angle-annular-dark-field-scanning-transmission electron microscope (HAADF-STEM). The one is the Pt clusters with size below 0.5 nm and the other is Pt nanoparticles with size up to 1.5 nm. The small Pt clusters are much smaller than commercial Pt catalysts. Due to more available surface area, these smaller nanoclusters of Pt/GNS improve methanol oxidation reaction (MOR) performance. The current density of Pt/GNS is about 0.6 mA/cm^2 at the over-potential of 0.6 V vs. RHE, which is better than commercial Pt/C. In addition, in the *i*–*t* curve result at 0.6 V vs. RHE for 30 min, the Pt/GNS showed a

4 times higher current density (0.12 mA/cm^2) than that of commercial Pt/C (0.03 mA/cm^2). The CO adsorption rate of Pt/GNS is extremely smaller by about 40 times less than that of Pt/C. This result represents the excellent CO poisoning tolerant of Pt/GNS.

Another example is that the high amount of Pt loadings as high as 80 wt% is able to be deposited onto the surface of the synthesized GNS without any assistance of surfactant [61]. The size dimension of Pt particles is less than 3 nm. The Pt/GNS catalysts with 40, 60 and 80 wt% Pt loadings have electrochemical active surface areas (ECSA) of 53, 51 and 36 m^2/g, respectively, while the conventional 40 wt% Pt/C catalyst has an ECSA of 26 m^2/g. In addition, all Pt/GNS catalysts exhibited much higher current densities for MOR than the commercial Pt/C. Specifically, the 60 wt% Pt/GNS showed approximately three times higher current density than that of the Pt/C, implying that the Pt/GNS in MOR performance is better than that of the conventional Pt/C.

Further works have demonstrated by Liu and coworkers [55]. Functionalized graphene sheets (FGSs) are prepared through a thermal expansion of GO. Pt nanoparticles with average diameter of 2 nm were then uniformly loaded on FGSs by impregnation methods. The Pt/FGS shows high initial current density and good retention on both the ECSA and ORR activity compared with the commercial Pt/C. After 5000 cycles, ECSA values of both Pt/FGS and commercial Pt/C have retained about 62.4 and 40%, respectively, of the initial values. Similarly in ORR activity, Pt/FGS retains 49.8% of its initial value, whereas the commercial Pt/C maintains 33.6%. Therefore, it is fair to say that Pt/FGS is much more stable than commercial Pt/C. After 5000 cycles, an average particle size of Pt/FGS is increased from 2 to 5.5 nm with more than 75% of Pt particles retaining its size below 6.9 nm. On the other hand, an average particle size of Pt/C is increased from 2.8 nm to 5.5 nm, and more than 45% of the particles have its size over 6.9 nm. The results indicated that the higher ECSA and ORR activity of Pt/FGS after durability test should be originated from maintaining smaller particle size in Pt/FGS.

Pt/rGO composites were also prepared *via* chemical reduction of GO and H_2PtCl_6 using $NaBH_4$ as reducing agent [47]. The ECSA of the Pt/rGO and commercial Pt/C are compared to be 44.6 and 30.1 m^2/g, respectively. The higher ECSA of Pt/rGO is favorable for MOR. The current density of Pt is determined to be 199.6 mA/mg at the potential of 0.652 V (vs. Ag/AgCl), while peak current density of commercial Pt/C is 101.2 mA/mg at 0.664 V. The Pt/rGO displays almost twice higher current density, but it has 12 mV lower over-potential than that of Pt/C. This result indicates that the performance of Pt/rGO for the MOR can be considered to be better than that of Pt/C.

Compared with Pt on activated carbon (Pt/C), the enhanced electrocatalytic activity of graphene supported Pt may be attributed to stronger interaction between flexible graphene sheets and Pt particles [47], which allows maintaining the smaller size of Pt particles and thus providing the larger ECSA.

Pt alloy/graphene hybrids

The bimetallic nanoparticles have attracted considerable interest due to their enhanced catalytic properties relative to individual nanoparticles [58]. Interestingly, compared with Pt/graphene, Pt-Ru/graphene, which are prepared in ethylene glycol solution [56], displays enhanced electrocatalytic activity for both methanol and ethanol oxidation. The tolerance against carbonaceous species such as CO can be assumed by the ratio of the forward anodic peak current density (I_F) to the reverse anodic peak current density (I_R). Figure 1 shows that Pt/graphene has the ratio of 6.52, which is much higher than Pt/carbon black (CB) (1.39) and Pt/graphite (1.03). This result demonstrates that Pt/graphene generates a more complete oxidation of methanol to CO_2. On the other hands, the methanol oxidation potential of Ru-Pt/graphene is shifted to 0.50 V compared with 0.65 V for Pt/graphene, which suggests that the addition of Ru can fairly improve the methanol oxidation, and thus Pt-Ru/graphene performs better catalytic activity than Pt/graphene. These effects ascribes that Ru-Pt alloys can effectively promote the complete oxidation of methanol to CO_2 producing less amount of CO and other carbonaceous species formed on their supports such as graphene, CB, and graphite electrodes. Similar with methanol, the Ru-Pt/graphene also shows significantly enhanced ethanol oxidation compared with other carbon supports.

Other similar work has demonstrated that graphene-supported Pt, Pt_3Co and Pt_3Cr alloy nanoparticles could be prepared by ethylene glycol reduction followed by pyrolysis at 300 °C [63]. The ECSAs are determined to be 65, 57 and 55 m^2/g for graphene-supported Pt, Pt_3Co and Pt_3Cr catalysts, respectively. The amount of oxide formation on these catalysts follows Pt, Pt_3Co and Pt_3Cr, ($Pt > Pt_3Co > Pt_3Cr$) in that order, because of the increased donor ability of Co and Cr [64,65]. This may have a beneficial effect on the oxygen enrichment of the ORR kinetics. The ORR activity of the graphene supported Pt_3Co and Pt_3Cr catalysts is increased about 3–4 times compared with graphene supported Pt. The higher activity of Pt alloys stems from the suppression of hydroxyl formation on Pt surface [63]. Moreover, the over-potential for ORR of the Pt alloys is 45–70 mV less than that of Pt. Hence, it can be concluded that the graphene supported Pt alloys improve the ORR activity and lower over-potential for ORR.

Some other bimetallic Pt-Pd/graphene enhances more catalytic properties relative to their individual nanoparticles. Wang and coworkers [58] demonstrated the synthesis of Pt-on-Pd bimetallic nanodendrites supported on graphene nanosheets (TP-BNGN) *via* wet-chemical approach. As shown in Figure 2, Pt nanobranches on Pd cores are directly grown onto the surface of graphene nanosheets with an average size of 15 nm. The ECSA of TP-BNGN (81.6 m^2/g) exhibits higher than those of Pt/C (54.7 m^2/g) and Pt/CB (19.2 m^2/g). This result should be originated from the particular structure of bimetallic nanodendrites and their better dispersion on the graphene nanosheets with a high surface area. The number of branches for Pt-on-Pd bimetallic nanodendrite on the surface of graphene nanosheets could be easily controlled by simply changing the reaction parameters, thus resulting in the tunable catalytic properties. The bimetallic nanodendrite/graphene hybrids exhibit about 3.0 and 9.5 times higher electrocatalytic activity for MOR than those of commercial Pt/C and Pt/CB catalysts.

A study on synthesis of the poly(diallyldimethylammonium chloride) (PDDA) mediated Pt-Au alloy nanoparticles

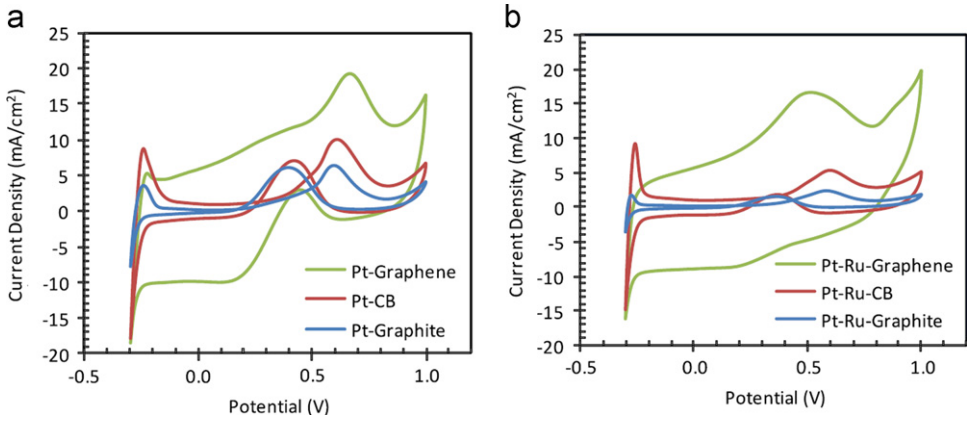

Figure 1 Cyclic voltammograms of (a) Pt nanoparticles and (b) Pt-Ru nanoparticles on different carbon-based supports in 1 M CH_3OH/0.5 M H_2SO_4 at 50 mV/s. Reprinted with permission from Ref. [56]. Copyright (2010) Elsevier.

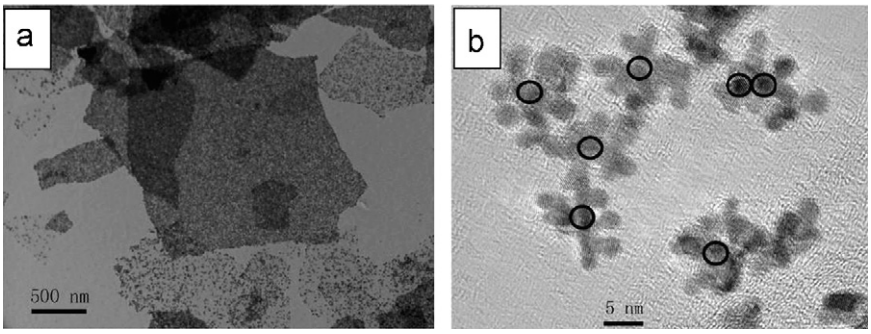

Figure 2 TEM (a) and HR-TEM (b) images of TP-BNGN. The circled parts in panel B denotes as Pd nanoparticles. Reprinted with permission from Ref. [58]. Copyright (2009) American Chemical Society.

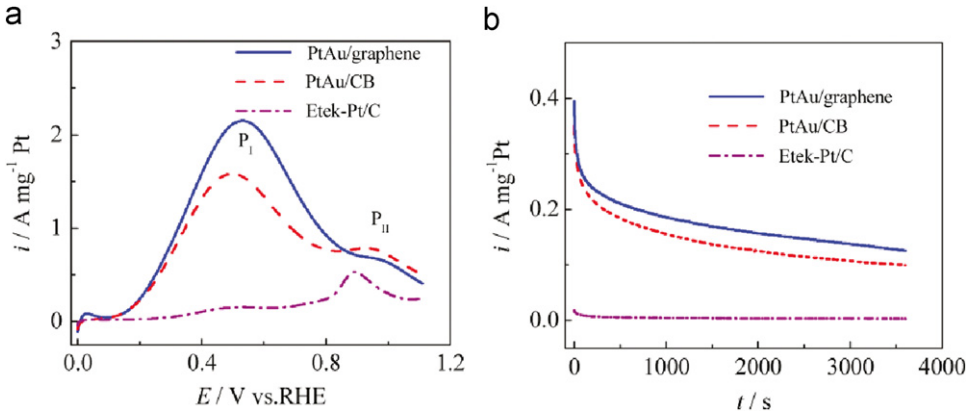

Figure 3 Formic acid oxidation (a) at the scan rate of 50 mV/s and amperometric *i*-*t* curves (b) at a fixed potential of 0.3 V on PtAu/graphene, PtAu/CB, and commercial Etek-Pt/C in N_2-saturated 0.5 M H_2SO_4+0.5 M HCOOH. Reprinted with permission from Ref. [66]. Copyright (2011) American Chemical Society.

loaded on graphene is carried out by Lin and coworkers [66]. PDDA has an important role as nanoreactors for the preparation of well-defined Pt-Au alloy nanoparticles and facilitates the uniform loading of Pt-Au alloys on graphene [67]. As shown in Figure 3a, the onset potential of formic acid oxidation on Pt-Au/graphene and Pt-Au/CB (170 mV) is much lower than commercial Etek-Pt/C catalyst (300 mV). The P_I peak is related to dehydrogenation reaction ($HCOOH \rightarrow CO_2 + 2H^+ + 2e^-$), while the P_{II} peak is contributed to the dehydration reaction ($HCOOH \rightarrow CO_{ads} + H_2O \rightarrow CO_2 + 2H^+ + 2e^-$) [68,69]. The intensity of P_{II} peak from Pt-Au/graphene is lower than that of Pt-Au/CB, which suggests that the formation of CO is smaller on Pt-Au/graphene. Thus, the presence of graphene in Pt-Au/graphene inhibits the CO poisoning during the formic acid oxidation. Therefore, the higher electrocatalytic activity of Pt-Au/graphene can be attributed to the strong interaction between graphene and Pt-Au alloy nanoparticles [47], which can minimize the CO poisoning and facilitate the direct formic acid oxidation on the Pt-Au surface. Furthermore, Figure 3b

shows the Pt–Au/graphene has best catalytic stability among tested samples toward formic acid oxidation.

In addition, ternary alloy systems have also been studied due to their superior catalytic activity and stability to binary alloys. Recently, Wang and coworkers [70] have prepared Pt-Pd-Au/rGO catalyst *via* simply ethylene glycol-water reduction from GO and Pt, Pd and Au precursor salts. The onset potential of MOR on Pt-Pd-Au/rGO shifted to the more negative values with decreasing the over-potential in the electrooxidation reaction. Moreover, the forward current density (I_f) of Pt-Pd-Au/rGO was 1.5, 2.3 and 2.8 times higher than those of Pt-Pd/rGO, Pt-Au/rGO and Pt/rGO, respectively. Compared with Pt-Pd/rGO and Pt-Au/rGO, the Pt-Pd-Au/rGO electrode shows (1) the lowest onset potential and (2) enormous current density of electrooxidation. The high catalytic activity of ternary system for MOR in alkaline is due to the combination of the third metal. As the scan rate and methanol concentration increased, the high MOR activity of Pt-Pd-Au/rGO catalysts is proven to be a diffusion controlled process on the basis of the linear relationship between the current density and the square root of scan rate.

The graphene supported Pt-based binary and ternary alloy electrocatalyst systems generally show more enhanced catalytic properties such as high electrocatalytic activity [66] and exhibit low over-potential for ORR (or MOR) owing to the combination of individual nanoparticles, which can inhibit aggregation of Pt particles. However, they consist of expensive noble metals and have still limited stability against intermediate species and anode crossover.

Heteroatom-doped carbon materials to replace Pt-based alternatives

Pt nanoparticles have long been regarded as the best catalyst for the ORR in fuel cells, although the Pt-based electrodes still have many problems such as time dependent drift, CO poisoning, high cost and limited reserves in nature. Hence, the development of nonprecious metal and/or metal-free ORR electrocatalysts has thus triggered a great deal of interest [51].

Although there are a numerous reports on those subjects [56–60,71], the heteroatom-doped graphene, nitrogen-doped graphene in particular, will only be discussed in this review considering space limit and relevant importance. The nitrogen-doped graphene (N-graphene) is synthesized by CVD of methane in the presence of ammonia [59]. The current density of metal-free N-graphene electrode exhibited to 3 times higher than commercial Pt/C electrode *via* 3.6–4 electron pathway in alkaline solutions. Compared with Pt/C, N-graphene shows not only stable amperometric response for ORR after the addition of hydrogen gas, glucose and methanol, but also long-term operation stability for 200,000 cycles and good tolerance against CO poisoning. The result indicates that N-graphene is readily promising material for ORR application with commercial versatility to replace problematic noble metal-based catalysts. As a result, together with its precedent N-doped vertically aligned carbon nanotube (N-VACNT) [51], N-graphene has paved the road for active researches on fuel cells.

Although N-graphene from CVD method has demonstrated the potential for metal-free electrocatalyst applications, mass production by CVD is limited. In this regard, N-graphene films are prepared by simple solution casting and heat-treatment of edge-selectively functionalized graphite (EFG) with 4-aminobenzoyl moieties [71]. The 4-aminobenzoyl moieties at the edges of EFG can be the *in-situ* feedstock for carbon and nitrogen sources for ''C-welding'' as well as ''N-doping'' at the same time. The EFG solution in NMP is dip-coated on a glassy carbon (GC) electrode. EFG/GC electrode is heat-treated at 900 °C for 3 h under an argon atmosphere to afford N-graphene/GC electrode and tested electrocatalytic activity. In cyclic voltammogram (CV) curve, the electrode does not show specific peaks in N_2 condition, while the oxygen reduction peak appeared at the potential of −0.15 V in O_2 saturated condition. The N-graphene/GC shows similar ORR catalytic activity to that of N-graphene prepared by CVD [59]. The nitrogen content of N-graphene from EFG is 1.7 at%, which is lower than the nitrogen content (4.0 at%) of the N-graphene from CVD [59]. The result is attributed to presenting many wrinkles (Figure 4) and the higher nitrogen concentration at welded boundary. The former produces a larger surface area and the latter provides more effective sites for efficient ORR activity.

In addition to N-doping level [72], the catalytic activity of N-graphene is also significantly related to the types of

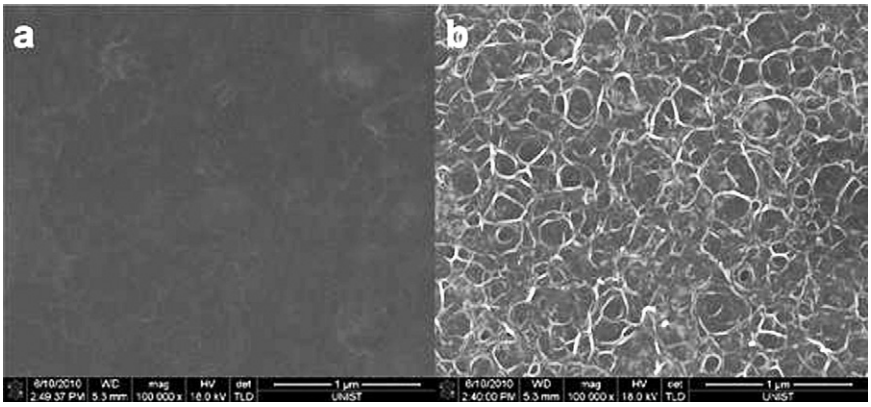

Figure 4 SEM images: (a) as-cast EFG film on silicon wafer by drop coating of EFG dispersed solution in NMP; (b) heat-treated EFG (N-graphene) film on silicon wafer at 900°C under an argon atmosphere. Reprinted with permission from Ref. [71]. Copyright (2011) American Chemical Society.

nitrogen in the carbon frameworks [60]. The rGO-based carbon nitride (CN) is obtained by using GO nanosheet on silica annealed at 800 °C under argon (G-CN800). The G-CN800 is not noticeably responded in O_2 saturated 0.1 M KOH solution with 3 M methanol. The result implies that G-CN800 nanosheets exhibit a high selectivity for ORR with a good tolerance of crossover effects, and thus it is superior to the commercial Pt/C catalyst. The onset potentials of G-CN nanosheets are more positive than CN nanosheets themselves, which suggest that graphene in nanosheets significantly affects their electrocatalytic behavior and over-potential of the electrodes. Furthermore, the G-CN800 nanosheets exhibit an efficient one step, four electron transfer pathway with a high kinetic current density of 7.3 mA/cm^2. This value is superior to that of commercial Pt/C with 5.4 mA/cm^2.

Dai and coworkers [57] have reported that hybrid material consisting of Co_3O_4 nanocrystals grown on rGO (CO_3O_4/rGO) and N-doped rGO denoted as Co_3O_4/N-rGO by adding NH_4OH during heat-treatment. They are used as high performance bifunctional catalysts for the ORR and oxygen evolution reaction (OER). As shown in Figure 5a, the Co_3O_4/rGO hybrid material showed a much more positive ORR onset potential (~0.88 V vs. RHE) and higher cathodic currents compared with Co_3O_4 and rGO alone. The electron transfer number of CO_3O_4/rGO is ~3.9 and CO_3O_4/N-rGO is ~4 from the slopes of Koutecky-Levich plots (Figure 5b, c). The CO_3O_4/N-rGO hybrid catalyst also exhibit excellent ORR activity (Figure 5d) with much smaller Tafel slope of 42 mV/decade at low over-potentials than that measured with CO_3O_4/rGO hybrid (54 mV/decade) in 0.1 M aqueous KOH solution. In 1 M and 6 M KOH electrolytes, the current density of CO_3O_4/N-rGO catalyst is similar to the performance of freshly loaded Pt/C catalyst, accompanied by a positive shift in the ORR onset potential from 0.1M KOH electrolyte. The Tafel slop of kinetic current is down to ~37 mV/decade for CO_3O_4/N-rGO in 1 M KOH, among the smallest Tafel slopes afforded by ORR catalysts. The CO_3O_4/N-rGO hybrid exhibits superior durability to Pt/C catalyst in 0.1–6 M aqueous KOH electrolytes, with little decay in ORR activity. On the other hand, the Pt/C catalyst exhibits 20–48% decrease in catalytic activity in 0.1–6 M aqueous KOH electrolytes, giving lower long-term ORR current than the stable currents sustained by the CO_3O_4/N-rGO. Pt catalyst is known to gradually degrade over time because of surface oxides and particle dissolution and aggregation, specifically

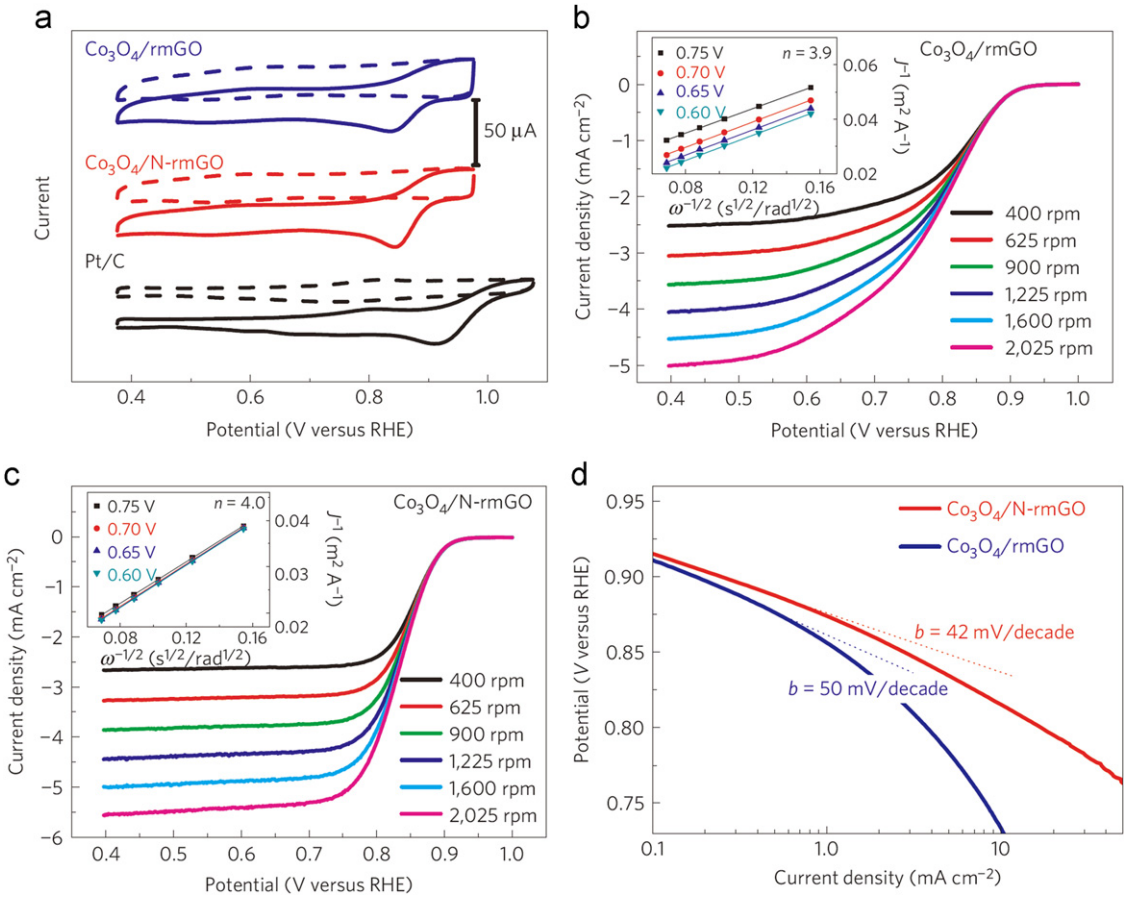

Figure 5 (a) *CV* curves of Co_3O_4/rGO hybrid, Co_3O_4/N-rGO hybrid and Pt/C on glassy carbon electrodes in O_2-saturated (solid line) or Ar-saturated 0.1 M aqueous KOH solution (dash line); (b) rotating-disk voltammograms of Co_3O_4/rGO hybrid; (c) Co_3O_4/N-rGO hybrid in O_2-saturated 0.1 M aqueous KOH solution with a sweep rate of 5 mV/s at the different rotation rates indicated. The insets in (b) and (c) show corresponding Koutecky-Levich plots (J^{-1} vs. $\omega^{-0.5}$) at different potentials; (d) Tafel plots of Co_3O_4/rGO and Co_3O_4/N-rGO hybrids derived by the mass-transport correction of corresponding RDE data. Reprinted with permission from Ref. [57]. Copyright (2011) Nature Publishing Group.

Table 2 Properties of graphene-based electrocatalysts.

Materials	Current density (mA/cm^2)	Onset potential (V)	ECSA (m^2/g)	Remark	Ref.
Pt/G	0.6 at 0.6 V	0.5 vs. RHE	-	DMFC	[62]
40% Pt/GNS	-	0.17 vs. Ag/AgCl	53	DMFC	[61]
Pt/G	199.6 mA/mg at 0.652 V	-	44.6	DMFC	[47]
Pt/G	-	-	108	PEMFC	[55]
Pt-Ru/G	16.5 at 0.5 V	-	-	DMFC	[56]
Pt_3Co/G	~3 at 0.85 V	0.97 vs. NHE	57	PEMFC	[63]
Pt_3Cr/G	~3.9 at 0.85 V	0.995 vs. NHE	55	PEMFC	[63]
PtAu/G	2.310 A/mg	-	-	DFAFC	[66]
PtPd/G	647.2 mA/mg	-	81.6	DMFC	[58]
PtPdAu/G	27.1	−0.642 V vs. SCE	-	DMFC	[70]
N-G	~−1.3 at 0.8 V	-	-	AFC	[71]
N-G	~−0.75 at 0.8 V	-	-	AFC	[59]
CN-G	7.3	-	-	DMFC	[60]
Co_3O_4/N-rmG	52.6	0.88 V vs. RHE	-	AFC	[57]

G: Graphene; N-G: N-doped grapheme; CN: carbon nitride; ECSA: electrochemically active surface area; DMFC: direct methanol fuel cell; PEMFC: polymer electrolyte membrane fuel cell; DFAFC: direct formic acid fuel cell; AFC: Alkaline fuel cell.

in the alkaline electrolytes used for alkaline fuel cells. As noble metals show poor catalytic durability for alkaline fuel cell, developing alkaline stable catalysts becomes one of the major challenges. The excellent stability of CO_3O_4/N-rGO hybrid envisions that it is promising candidate for ORR and other important catalytic reaction in alkaline solutions. The water oxidation regime and electocatalytic oxygen evolution reaction (OER) are performed in 0.1 M aqueous KOH solution. The CO_3O_4/N-rGO hybrid shows a current density of 10 mA/cm^2 at a small over-potential of ~0.31 V and a small Tafel slope down to 67 mV/decade, whose values are comparable to the performance of the best reported CO_3O_4 nanoparticle OER catalyst at the same loading. The electrochemical characteristics of representative graphene-based catalysts are summarized in Table 2, in which the properties of graphene based electrocatalysts have been tried to improve their catalytic performance. Thus, the commercial Pt-based catalysts, which are cost inefficient and poor intermediate tolerance, are expected to be replaced. The performance can be judged by three different factors: higher current density, lower onset potential and higher ECSA compare with Pt/C. The catalysts were categorized by the materials, which are using a less amount of Pt, Pt alloy and metal-free catalysts.

Capacitors

Background

Energy paradigm has been changing, which generally includes the recognition of energy, pattern of consuming energy, the role of industry structure and its values. Many scientists have suggested and developed the new paradigm, which occurred by the complicated problems such as petroleum exhaustion, environmental pollution, green house effect and climate change. Future energy paradigm will include concepts that diminishing wasteful energy, enriching the life style and not burdening environment. The first assignment for a human being is the displacement of current energy to new sustainable energy resources and more efficient use. Supercapacitors are going to pave the way to one of new sustainable energy paradigm.

Supercapacitors, also called ultracapacitors, store electrochemical energy by accumulating the charge from electric double layer, which is caused by electrostatic attraction. The capacity of supercapacitor is proportional to the electrode surface, i.e., the electrochemically active surface, where how much ions are attracted. As mentioned earlier, it is a different from physically determined surface area by nitrogen physisorption [73]. Electrochemical capacitors (EC) are possible to be fully charged and discharged in seconds. Although their energy density (about 5–10 W h/kg) is lower than in batteries or fuel cells, higher power density (10 kW/kg) can be reached in a short time [74]. The most attractive advantage of ECs is a high power capability with the fast charge/discharge rate. Moreover, most of the ECs are safer against short circuit than batteries in terms of the possibility of self-ignition. They do not contain any hazardous or toxic materials and have the durability during long charge–discharge cycles [75].

There are two representive mechanisms describing the supercapacitor: (1) electric double layer capacitor (EDLC) and (2) psuedocapacitor. EDLCs store the charge electrostatically following to reversible adsorption–desorption cycles of electrolyte ions onto active electrode materials (Figure 6). The active materials should not only be electrochemically stable, but also have accessible large surface area. Furthermore, there should not be Faradaic reaction at EDLC electrode. Surface storage mechanism allows very fast energy uptake and delivery, and better power performance. However, the physicochemical process and electrode polarization in EDLC are not enough to apply high energy devices. Pseudocapacitors, on the other hand, undergoe reversible Faradaic reactions. Chemically modified carbon materials [76,77], metal oxide [78] and conducting polymers [79,80] are used for electrodes. In cases of pseudocapacitors, the stability for charge/discharge cycling is relatively poor, though their energy densities are relatively high with respect to EDLCs. Furthermore, the response time is longer than EDLCs, because it takes longer time to move electrons during the redox reaction [81].

In order to control the performance of supercapacitors, the major factors such as electrolyte, separator thickness, and properties of electrode including porosity, mechanical stability, volume, resistance, etc., need to be considered [75]. Graphene is known to be emerging material for supercapacitor applications, due mainly to its superb properties to conventional carbon-based materials. Graphene meets the requirements for electrode material in supercapacitor: graphene has the large surface area (2630 m^2/g) [82], good thermal [11] and electrical conductivity (4840-5300 W/m K, 2×10^2 S/m) [82], theoretical double layer capacitance (~21 $\mu F/cm^2$) [83]. Theoretically large surface area of graphene provides electroactive site and easy to accessibility to electrolyte ions, and good electrical conductivity can reduce the resistance of transportation of electron, especially for pseudocapacitor. Graphene has shown promising electric properties for supercapacitor. In addition, composites, consisting of graphene with other electrode materials such as activated carbon [84], metal oxide [42,85] and conducting polymer [86,87], could be expected to show synergetic effects on supercapacitors (Table 3).

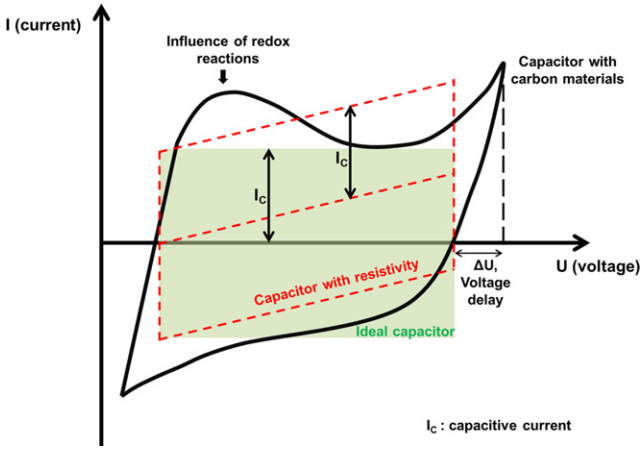

Figure 6 Typical charge/discharge voltammetry characteristics of an electrochemical capacitor. Reproduced with permission from Ref. [81]. Copyright (2001) Elsevier.

Materials based on graphene

Reduced GO (rGO)

Curved morphology of rGO was measured an energy density of 85.6 Wh/kg at 1 A/g and the power density of about 9.8 kW/kg at 8 A/g in ionic liquid, EMIM/BF_4 [89]. Curved morphology caused by the convection dry process and has the mesoporous structure. The morphology of surface area is important to make electric double layer from diffusion of ions. The ionic liquid is possible to form higher EDLC than aqueous electrolyte and operating voltage over 4 V even if ionic liquid is bulky and viscous [89].

The graphene exfoliation was succeeded at 200 °C as relatively low temperature with high vacuum. The specific capacitance is 279 F/g in scan rate 10 mV/s in 30% KOH solution. The oxygen content is different between high temperature (C/O ratio 11:1) and low temperature processes (C/O ratio 10:1). It implies that different surface chemistry leads to different electrochemical performances [98].

The other way to produce the graphene electrode is the microwave treatment with KOH activation used to improve porosity and enhanced supercapacitor performance. This product had a large surface area around 3100 m^2/g from BET measurement. In the BMIM BF_4/AN electrolyte, this product has the specific capacitance 166 F/g and shows stable state after 10,000 charge/discharge cycles as having the capacitance retention of 97%. Above all, the energy

Table 3 Overview of graphene materials with capacitor's properties.

Materials	Treatment	Power density (kW/kg)	Energy density (W h/kg)	Specific capacitance (F/g)	Ref.
Graphene	CVD (chemical vapor depostion)	-	-	80 F/cm^2	[88]
rGO	Reduced graphene and convection dry	9.8	85.6	250	[89]
Functionalized GO	Thermal exfoliation of graphite oxide	-	28.5	230	[90]
N-doped graphene	N_2 plasma	800	48	282	[91]
Carbon black-graphene	Ultrasonication and *in situ* reduction process	-	-	175	[84]
CNT-graphene	CVD	-	-	385	[92]
Carbon sphere-GNS	Self-assemblly chemical reduction	15.4	-	198	[93]
PANi-graphene	*In situ* polymerization	0.14	37.9	1126	[87]
PPy-Graphene	Electric depostion on graphene oxide	3	5.7	1510	[86]
PEDOT-graphene	Oxidative polymerizaiotn	0.038	12	304	[94]
MnO_2-exfolitated graphite	Dip and dry deposition	110	12.5	315	[95]
RuO_2-graphene	Sol-gel process with RuO_2 and graphene oxide	0.05	20.1	570	[42]
NiO-graphene	Electrophoretic deposition and chemical bath deposition	-	-	400	[96]
Fe_3O_4-graphene	Crystalization of metal oxide with rGO	2.4	85	326	[97]

density is ~70 W h/kg, which is about four times higher than energy density of activated carbon electrodes and nearly equal to that of lead hybrid [44].

Yoo et al. designed 2D plane ideally to utilize the high surface area of graphene and simply fabricated the electrode. They synthesized rGO CVD film and tested in solid electrolyte, polymer-gel (PVA-H_3PO_4). The electrode showed the specific capacitance around 250 F/g with good cycle stability up to 3000 charge/discharge cycles [88].

Graphene hydrogel made of hydrothermal reduction of GO, and using hydrazine monohydrate and hydroiodic acid as reductants. Hydrothermal reaction produces strongly cross-linked 3D graphene network by overlapping graphene sheets. This reducing process increases hydrophobicity and the π-conjugation length of graphene [99]. This rGO has micrometer pores and specific surface area of 778–964 m^2/g. The rGO by hydrazine monohydrate has the specific capacitance of 220 F/g at a current density of 1 A/g, the power density of 30 kW/kg and the energy density of 5.7 W h/kg [100].

Nitrogen doped graphene

Heteroatom doping to the graphitic framework leads to changes of structures, thermal and electric properties and Fermi level [101]. Nitrogen doped graphene (N-graphene), in particular, could simply be prepared by nitrogen plasma treatment [102]. N-graphene has shown the better electrode capability than graphene [102]. Choi and coworkers [91] are able to dope nitrogen into the graphene basal planes *via* simple nitrogen plasma process. They measured the specific capacitance of 282 F/g, which were 4 times higher compared to pristine graphene, whose capacitance was 68 F/g in organic solvent electrolyte [91]. By simple replacement of the carbon atoms with nitrogen atoms from the basal plane of graphene, N-graphene based supercapacitor maintains 99.8% of capacitance after 100,000 cycles [91]. The power and energy densities have been achieved up to $\sim 8 \times 10^2$ kW/kg and ~48 W h/kg, respectively, in 1 M tetraethylammoniumtetrafluoroborate (TEA BF_4) [91]. The rGO, reduced by hydrazine and subsequent annealing in NH_3 atmosphere, has produced N-graphene. The N-graphene displays maximum capacitance of 144.9 F/g at a current density of 0.5 A/g in conventional organic solvent-based electrolyte (Figure 7) [103].

Carbon material-graphene composites

Li and coworkers have synthesized self-assembled hierarchical nanostructure by electrostatic interaction between the two carbon spheres and graphene nanosheets [93]. The functionalized carbon spheres effectively separate graphene sheets preventing aggregation and its unique structure is used as active material to construct supercapacitors. The specific capacitance of the hierarchically nanostructured carbon sphere-graphene electrode is 198 F/g, which is higher than that of graphene electrode (115 F/g) and carbon sphere electrode (38 F/g). The cycle stability of hierarchical

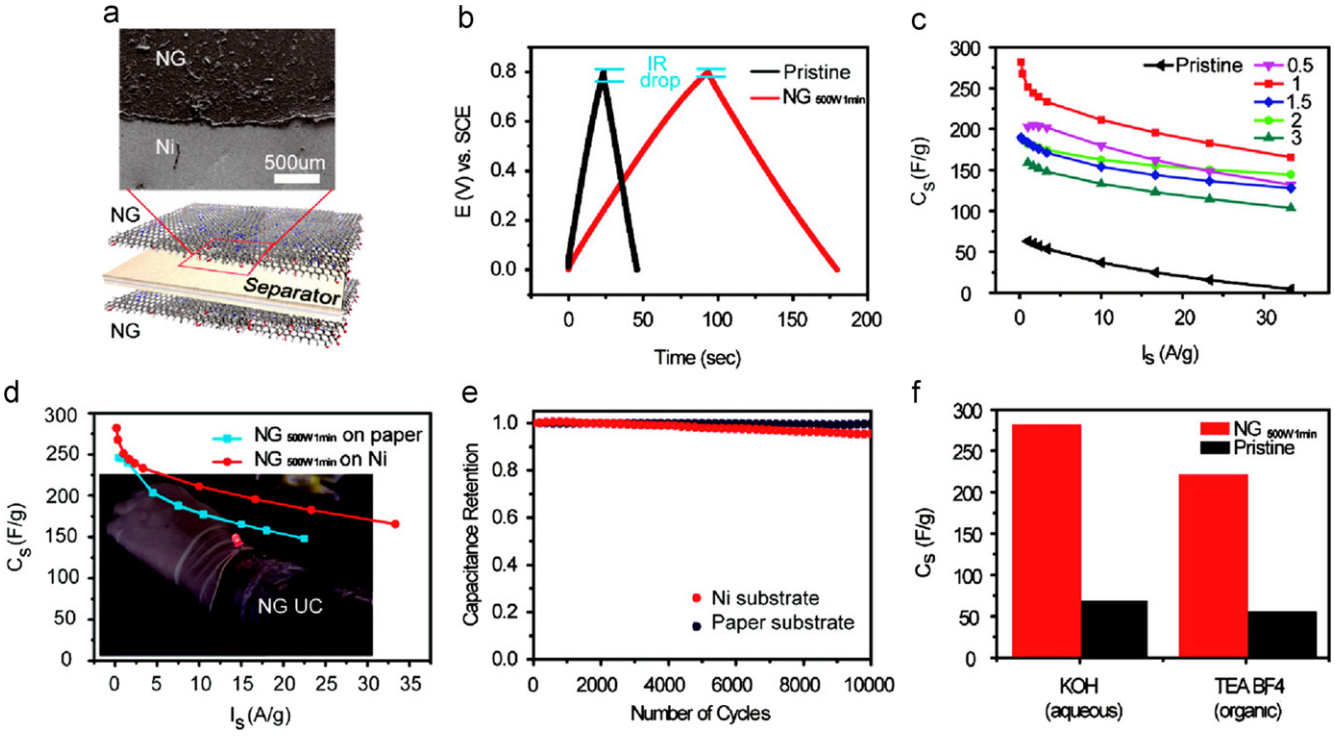

Figure 7 Ultracapacitors based on N-graphene and their electrochemical testing: (a) a schematic illustration of the assembled ultracapacitor structure; (b) charging and discharging curves measured by galvanostatic characterization; (c) gravimetric capacitances of ultracapacitor based on various N-graphene and pristine graphene measured at a series of current densities. The numbers in the legend indicate the plasma durations in minutes; (d) gravimetric capacitances of ultracapacitor built on nickel and paper substrates measured at a series of current densities; (e) the cycling tests for the ultracapacitor based on Ni and paper substrates up to 10,000 cycles; (f) the specific capacitances measured in aqueous and organic electrolytes. Reprinted with permission from Ref. [91]. Copyright (2011) American Chemical Society.

nanostructure is well retained up to more than 95% after 1000 charge/discharge cycles. Previously, graphene/CNT hybrid film were synthesized *via* self-assembly between poly(ethyleneimine) (PEI) functionalized graphene and acid treated CNT [104]. Heat treated graphene/CNT film on ITO glasses were obtained in 1 M H_2SO_4. The capacitance of graphene/CNT film is 120 F/g with rectangular shape, corresponding to well charging and discharging with low resistance on electrode.

Furthermore, three dimensional CNT/graphene sandwich (CGS) structure was prepared with CNT column grown on the graphene layers in the presence of Co catalysts by CVD method [88]. The CV curves of CGS exhibits strong redox peaks within potential range from −0.2 to 0.45 V in 6 M KOH solution. The result implies the high pseudocapacitance of $Co(OH)_2$. The CGS shows the capacitance of 385 F/g, which are higher value compare with CNT/graphene (physical mixing), graphene and Co_3O_4/graphene. This result should be originated from unique structure of CGS, which facilitated fast transport of the electrolyte ions or electron across the electrode matrix. To test the electrochemical stability of CGS, CV was measured 2000 cycles and initial capacitance is rather increased approximately 20% owing to increase of interfacial area between $Co(OH)_2$ and electrolyte during process, indicating excellent stability. In a similar, but independent study, Feng et al. [105] prepared 3D pillared vertically-aligned CNT-graphene architectures by intercalated growth of vertically aligned CNTs into thermally-expanded highly ordered pyrolytic graphite (HOPG). The resulting graphene and vertically-aligned CNT hybridized with nickel hydroxide coating showed a high specific capacitance (1065 F/g) with a remarkable rate capability.

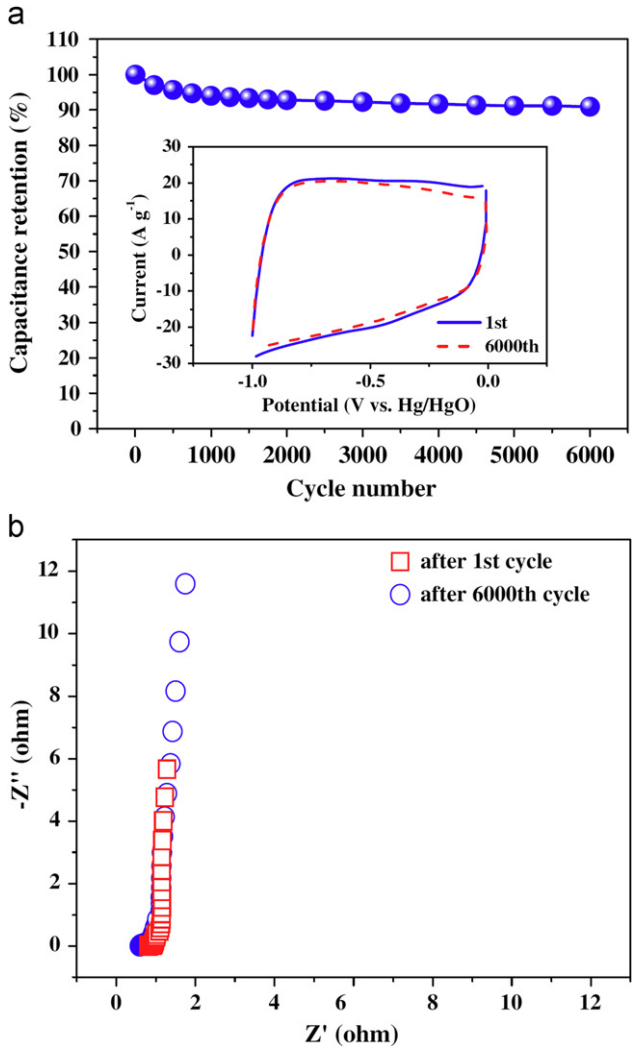

Figure 8 (a) The capacitance of GNS/CB-2 composite as a function of cycle number measured at 200 mV/s in 6 M aqueous KOH solution. Inset shows the *CV* curves of the 1st and the 6000th cycles at 200 mV/s. (b) Nyquist plots of GNS/CB-2 electrode in the frequency range of 100 kHz–0.1 Hz measured during the cycle life testing. Reprinted with permission from Ref. [84]. Copyright (2010) Elsevier.

Liu group also prepared graphene nanosheet (GNS)/carbon black (CB) composites by the ultrasonication and *in situ* reduction methods [84]. In case of the GNS/CB-1, mostly CB particles are deposited on to the basal plane of GNS, while GNS/CB-2, CB particles are located at the edges of GNS. The CV data show GNS/CB-2 has higher capacitance (175 F/g) with rectangular shape than those of GNS/CB-1 (150.4 F/g) and GNS (122.6 F/g), indicating that electrolyte ions diffusion and migration into GNS/CB-2 are more efficient than GNS/CB-1 during fast charge/discharge process. To estimate the long-term cycle stability of GNS/CB-2, not only CV was measured for 6000 cycles in the potential range from −1 to 0 V (vs. Hg/HgO) but also electrochemical impedance spectroscopy was tested in range of 100 kHz to 0.1 Hz. Figure 8 shows that the capacitance of GNS/CB-2 after 6000 cycles is diminished only 9.1% of initial value and impedance spectra well retained initial curve, meaning that CNS/CB-2 has excellent stability.

The carbon materials such as CB, CNT and carbon sphere can also act as spacer, therefore, enhanced the electrochemical properties through not only the increased surface area of carbon material/graphene composites, but also rapid transport of the electrolyte ions or electron across the electrode matrix.

Psudocapacitors: graphene/conducting polymer composites

Conducting polymers such as polyaniline (PANi), polypyrrole (PPy), polythiophene (PT), etc., have been utilized as base materials for multifunctional composites, which display enhanced properties such as structural reinforcement and electrical conductivity [106–108].

The addition of a small amount of GO into PANi enhanced specific capacitance as high as 531 F/g in the 1 M H_2SO_4 electrolyte (Figure 9). In addition, the conductivity was ascended over pure GO and PANi. The enhancement should be attributed to π-π stacking between PANi backbone and GO nanosheets [46]. Cheng et al. [109] fabricated GO/PANi composite by *in situ* anodic electropolymerization of aniline monomers into a PANi film on graphene paper. The specific capacitance of 233 F/g is abtained in the 1 M H_2SO_4 electrolyte. This electrode is stable at cycle test as shown in Figure 9d and its mechanical strength is improved by 43% [109].

Another graphene/PANi hybrid material, formed by three steps of *in situ* polymerization-reduction/dedoping-redoping process, renders the high specific capacitance as high as 1126 F/g at a scan rate 1 mV/s. Specific energy density and

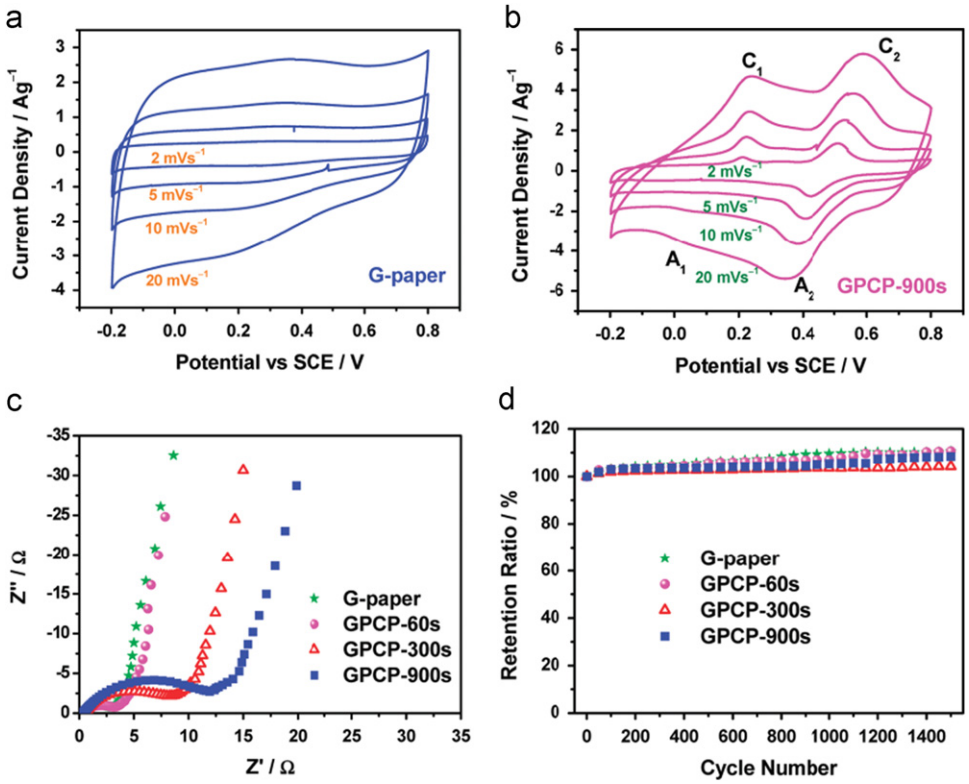

Figure 9 Electrochemical properties of the graphene-paper (G-paper) and graphene-PANi composite paper (GPCP): (a,b) cyclic voltammograms recorded from 2 to 20 mV/s in 1 M H_2SO_4; (c) Nyquist plots of the G-paper and GPCP-60 s/300 s/900 s (different deposition time); (d) cycling stability measured at 50 mV/s. Reprinted with permission from Ref. [109]. Copyright (2009) American Chemical Society.

power density are 37.9 Wh/kg and 141.1 W/kg, respectively [87]. The rGO/PANi (PANi ratio, 5 wt%) also exhibits good performance with specific capacitance of 480 F/g at 0.1 A/s. The rGO/PANi composite electrodes have generally higher specific capacitance and conductivity than those of GO/PANi composite electrode. GO typically has insulating characteristics due to topological defects and numerious oxygenated groups. Although initial capacitance of graphene/PANi composites as psudosupercapacitor electrodes are much higher than that of just carbon-based electrodes, cycle stability is generally very poor [110]. The electrochemical instability is because of defects creation by swelling, shrinkage and cracking during charge/discharge cycles.

PPy, one of the conducting polymers, has some advantages for psudosupercapacitor materials. It can be produced at low cost and has high specific capacitance, ease to process in water solution and fast electrochemical switching [111]. GO/PPy composite has been prepared by electrophoretic deposition on titanium substrate. This electrode displays the specific capacitance of 1510 F/g at a scan rate of 10 mV/s in 0.1 M aqueous $LiClO_4$ electrolyte. The outstanding performance is stemmed from the cohesive network structure between graphene and PPy. Although most of conducting polymers show poor cycle stability, this electrode is relatively stable. Energy density and power density are 5.7 W h/kg 3 kW/kg, respectively [86]. Other method to prepare GO/PPy flexible film is pulsed electrochemical deposition [112]. The amount of PPy on the GO surface depends on the deposition time. The specific capacitance is 237 F/g in 1 M aqueous KCl solution, when deposition time is 120 s. Both ionic diffusion resistance and charge-transfer resistance are related to particle size and amount of PPy. In this case, the energy and power densities are 33 Wh/kg and 1.18 kW/kg, respectively, at a scan rate 10 mV/s [112].

Polyethylenedioxythiophene (PEDOT)/polystyrene sulfonate (PSS) mixture is well known conducting polymer system. Graphene-PEDOT (G-PEDOT) composite is synthesized by oxidative polymerization in the presence of graphene. The composite displays the maximum capacitance of 374 F/g at a scan rate of 0.01 A/g. Owing to doping/dedoping process being involved in the charge transportation and ion transportation, G-PEDOT has the power density of 38 W/kg and the energy density of 12 Wh/kg [94].

Psudocapacitors: graphene/metal oxide composites

Similar to conducting polymers as organic materials, metal oxide electrodes as inorganic materials enable to improve the capacitance through pseudocapacitance effects originated from the redox behaviors. However, the weakness of metal oxides is limited electrical conductivity. In this sence, graphene could provide conductive pathway in graphene/metal oxide composites. The interaction between graphene and metal oxide is prone to improve supercapacitor performance. Metal oxides palys as not only spacer to expand the surface area of graphene but also its redox reaction to add more capacitance. The expanded surface of graphene makes ions

easy to diffuse and provides conductive channel for efficient electron transfer by reducing the resistance [113].

Manganese oxide (MnO_2) has been demonstrated to be one of the promising psuedocapacitor electrodes, because of its low cost, environmental friendly material, and high theoretical capacitance. It is able to deliver high specific capacitances ranging from 700 to 1380 F/g, when MnO_2 is deposited with a few hundreds nanometer thickness. However, commercial MnO_2 film capacitors have the specific capacitance of 150–250 F/g. Due to the formulation consisting of carbon materials, binders and MnO_2 has micrometer thickness and thus they have low surface area to access and poor electrical conductivity [114]. Various kinds of hybrid composites are suggested to solve this problem arising from limitation of thickness and fully utilize the advantage of MnO_2 [115].

GO/MnO_2 composite has been prepared by a simple solution process. Oxygenated groups on the GO surface provide anchor sites to grow needle-shaped MnO_2 crystalline at low temperature. Synergistic effect from GO and MnO_2 has been observed, showing the specific capacitance of 197.2 F/g in the 1 M aqueous Na_2SO_4 solution and capacitance retention of about 84% after 1000 cycles [116].

Graphene sheets, obtained from exfoliated graphite by sonication, were coated on the polyester microfiber *via* dip and dry process. MnO_2 has been deposited on the graphene coated fiber *via* electrodeposition [85]. This composite has the specific capacitance of 315 F/g at a scan rate 2 mV/s, high stability up to 95%, power density of 110 kW/kg, and energy density of 12.5 W h/kg. Enhanced performance should stem from graphene coating on microfiber textile forming desirable interfacial contact with MnO_2 by expanding the surface area and conductive pathways. Furthermore, flower-like MnO_2 crystals have increased electrochemically active site, enahnced charge transfer and reduced diffusion length during charge/discharge process [85]. As a result, it is expected to further boost overall electrochemical properties by wrapping conductive polymer mixture, PEDOT:PSS, in this system. In this case, the specific capacitance is achieved maximum 380 F/g at a current density of 0.1 mA/cm^2 [95]. The rGO/MnO_2 composite is also synthesized by redox reaction with assistance of microwave irradiation to combine them more rapidly [115]. The electron transfer reaction between graphene as reduction reagent and metal oxide as oxidant facially and rapidly occurred to achieve the specific capacitance of 310 F/g and capacitance retention up to 95.4% after 15,000 cycles [115].

Other graphene-based metal oxide composites with zinc oxide (ZnO) and tin oxide (SnO_2) have also been synthesized by ultrasonic spray pyrolysis [117]. Graphene/ZnO and graphene/SnO_2 composites show specific capacitances of 61.7 and 42.7 F/g, respectively, at a scan rate of 50 mV/s. At the same scan rate, power densities are 4.8 kW/kg and 3.9 kW/kg in that order. Considering the power density of graphene itself is 2.5 kW/kg, graphene/metal oxide composites can drastically enhance their power densities [117]. The rGO/SnO_2 composite has also been produced by *in situ* reduction of GO in the presence of $SnCl_4$ in one-pot process. The capacitance of resultant composite is 43.4 F/g at a scan rate 1.0 V/s in 1 M aqueous H_2SO_4 solution [118]. The value is relatively poor compared with precedent graphene/metal oxide composites. In the case of rGO/ZnO composite system, the ratio between rGO and ZnO is sensitive factor for the electrochemical performances. When the rGO/ZnO composite was prepared from GO, the best mass ratio of GO to ZnO is 93.3 to 6.7. The composite displays the highest specific capacitance of 308 F/g at 1 A/g [119].

Although it is expensive because limited reserve of noble metal in the earth, hydrous ruthenium oxide (RuO_2) is known to posess a good cycle stability and high capacitance [120]. Graphene/RuO_2 sheet has been fabricated by sol–gel process, expecting RuO_2 particles anchored on the plane graphene surface (Figure 10). The specific capacitance of the graphene/RuO_2 with 38.3 wt% of RuO_2 is as high as 570 F/g with pseudocapacitor characteristics. The energy density is 20.1 W h/kg and the corresponding power density is 50 W/kg at 0.1 A/g. The energy density of composite is close to RuO_2 (22.2 W h/kg) and much higher than graphene sheet (3.1 W h/kg) [42]. Similar to rGO/PANi composite, rGO/RuO_2 shows the synergistic effect to strengthen the performance of capacitor. When rGO/RuO_2 composite with a loading RuO_2 amount of 17 wt% was used as a symmetric electrode, the energy density is 12.4 W h/kg; similar to rGO/PANi composite (13.9 Wh/kg). Interestingly, when those two composite electrodes are used as asymmetric electrode, the energy density of system is doubled to be 26.3 W h/kg at the current density of 0.3 A/g [121].

Cobalt hydroxide ($Co(OH)_2$) electrode has even higher capacitance than the noble and expensive RuO_2 electrode. Hence, GO/$Co(OH)_2$ composite (the optimum ratio is 1/30) attract more interest in supercapacitor application. The composite displays very high specific capacitance of 972.5 F/g at a current density of 0.5 A/g. The role of graphene sheets is impeding the agglomeration of $Co(OH)_2$ particles. As a result, the higher $Co(OH)_2$ feed ratio (below 1/50 for GO/$Co(OH)_2$) results in decreased specific capacitance, because excessive Co^{2+} in solution is aggregated and hinders dispersing $Co(OH)_2$ particles uniformly [122].

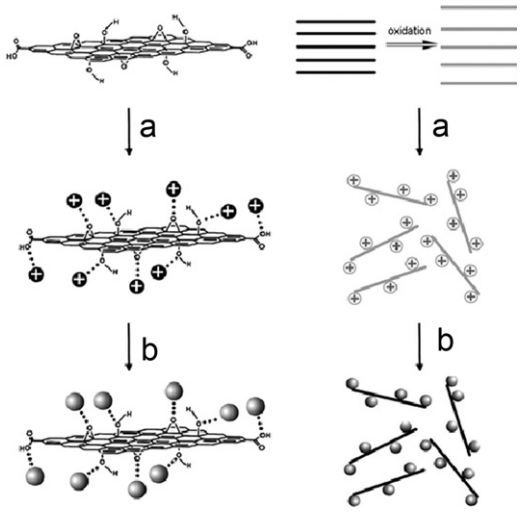

Figure 10 The formation process of graphene—$Co(OH)_2$ nanocomposites: (a) interactions between GO and Co^{2+} and (b) deposition of Co^{2+} and deoxygenation of GO at the same time. Reprinted with permission from Ref. [122]. Copyright (2010) American Chemical Society.

GO/cobalt oxide (Co_3O_4) composite has also been synthesized rapidly using microwave. The specific capacitance of GO/Co_3O_4 composite shows the specific capacitance of 243.2 F/g at 10 mV/s in 6 M aqueous KOH solution and maintaining the specific capacitance of 95.6% after 2000 cycles [123].

By morphology control, graphene/porous nickel monoxide (NiO) hybrid film displays pseudocapacitance of 400 F/g at 2 A/g. As compared with the specific capacitance (279 F/g at 2 A/g) of porous NiO film, graphene/NiO hybrid film has been profoundly improved capacitance due to its redox behavior. Graphene sheets play as reductant and help the oxidation of NiO film improving the electrochemical activity of the reversible reaction between Ni^{2+} and Ni^{3+} ions [96].

The rGO/nickel-covalt oxide ($NiCo_2O_4$) was prepared from self-assembly process. The redox couples of Co^{2+}/Co^{3+} and Ni^{2+}/Ni^{3+} coexist in this system, showing the initial specific capacitance of 835 F/g at 1 A/g. After 450 cycles, the specific capacitance soars to 1050 F/g implying that additional cycles are needed to fully activate the composite. The composite remains stable even after 4000 cycles [124].

By using commercialized iron oxide (Fe_3O_4), rGO/ Fe_3O_4 was prepared by crystallization of Fe_3O_4 in the presence of rGO. Considering the low cost of Fe_3O_4, this system has high potential for commerciallization with the specific capacitance 326 F/g at a current density 0.5 A/g. Its energy density and power density are 85 Wh/kg and 2.4 kW/kg, respectively [97]. In addition, GO/bismuth oxide (Bi_2O_3) was also produced *via* the solvothermal synthesis and demonstrated to have a reasonable specific capacitance of 222 F/g at 1 A/g [113].

Conclusions

Searching for new sustainable energy is a global issue given the likely depletion of current resources. Recently, researchers are showing much interest in graphene based study for energy devices, such as fuel cells and capacitors. Because graphene has been demonstrated to possess a good electrical conductivity and high surface area due to its unique 2-D structure, it is expected to be one of the best suitable base-materials for developing alternative energy sources. In this review, a recent significant progress in grpahene-based energy systems is summaized by presenting some representive examples, which can be listed as follows: (1) graphene supported Pt, Pt alloy and graphene-based metal-free catalysts have demonstrated enhanced electrocalytic acitivy with cycle stability for fuel cells, and (2) introduction of graphene as rGO, nitrogen-doped graphene, graphene/carbon material composites, grapehne/polyemr composites, and graphene/metal oxide composites display better power density, energy density and capacitance for capacitiors. These new hybrid materials have proven to demonstrate superb potential for commercialization viability over noble metal-based expensive catalysts and conventional capacitors. However, there are still big rooms in energy conversion and storage systems for further improvements in terms of overall performance and scalable low-cost production. We hope this review can provide valuable insights to reserchers for gain further knowledge to speed up novel innovation in this area. There should be bright future and no speed limit on grpahene-way for new energy sources.

Acknowledgements

This research was supported by WCU (World Class University), US-Korea NBIT and BRL programs through the National Research Foundation (NRF) of Korea funded by the Ministry of Education, Science and Technology (MEST), and the US Air Force Office of Scientific Research through the Asian Office of Aerospace R&D (AFOSR-AOARD).

References

[1] J.B. Hou, Y.Y. Shao, M.W. Ellis, R.B. Moore, B.L. Yi, Physical Chemistry Chemical Physics 13 (2011) 15384–15402.
[2] K.S. Novoselov, A.K. Geim, S.V. Morozov, D. Jiang, Y. Zhang, S.V. Dubonos, I.V. Grigorieva, A.A. Firsov, Science 306 (2004) 666–669.
[3] A. Peigney, C. Laurent, E. Flahaut, R.R. Bacsa, A. Rousset, Carbon 39 (2001) 507–514.
[4] A.K. Geim, K.S. Novoselov, Nature Materials 6 (2007) 183–191.
[5] T. Braun, M. Wohlers, T. Belz, G. Nowitzke, G. Wortmann, Y. Uchida, N. Pfänder, R. Schlögl, Catalysis Letters 43 (1997) 167–173.
[6] A. Pandolfo, A. Hollenkamp, Journal of Power Sources 157 (2006) 11–27.
[7] Y. Hwang, J. Lee, C. Lee, Y. Jung, S. Cheong, C. Lee, B. Ku, S. Jang, Thermochimica Acta 455 (2007) 70–74.
[8] P. Kim, L. Shi, A. Majumdar, P. McEuen, Physical Review Letters 87 (2001) 215502-215505.
[9] D. Menard, X. Py, N. Mazet, Chemical Engineering and Processing: Process Intensification 46 (2007) 565–572.
[10] H. Fukushima, L. Drzal, B. Rook, M. Rich, Journal of Thermal Analysis and Calorimetry 85 (2006) 235–238.
[11] A.A. Balandin, S. Ghosh, W.Z. Bao, I. Calizo, D. Teweldebrhan, F. Miao, C.N. Lau, Nano Letters 8 (2008) 902–907.
[12] S. Kobayashi, T. Takenobu, S. Mori, A. Fujiwara, Y. Iwasa, Applied Physics Letters 82 (2003) 4581–4583.
[13] T. Dürkop, S. Getty, E. Cobas, M. Fuhrer, Nano Letters 4 (2004) 35–39.
[14] M.S. Dresselhaus, G. Dresselhaus, Advances in Physics 30 (1981) 139–326.
[15] K.S. Novoselov, A.K. Geim, S.V. Morozov, D. Jiang, M.I. Katsnelson, I.V. Grigorieva, S.V. Dubonos, A.A. Firsov, Nature 438 (2005) 197–200.
[16] Y.B. Zhang, Y.W. Tan, H.L. Stormer, P. Kim, Nature 438 (2005) 201–204.
[17] A.A. Kolomenskii, M. Szabadi, P. Hess, Applied Surface Science 86 (1995) 591–596.
[18] R.H. Baughman, C. Cui, A.A. Zakhidov, Z. Iqbal, J.N. Barisci, G.M. Spinks, G.G. Wallace, A. Mazzoldi, D. De Rossi, A.G. Rinzler, Science 284 (1999) 1340–1344.
[19] J. Wu, D. Chung, Carbon 40 (2002) 445–446.
[20] L. Schadler, S. Giannaris, P. Ajayan, Applied Physics Letters 73 (1998) 3842.
[21] C. Lee, X.D. Wei, J.W. Kysar, J. Hone, Science 321 (2008) 385–388.
[22] R.R. Nair, P. Blake, A.N. Grigorenko, K.S. Novoselov, T.J. Booth, T. Stauber, N.M.R. Peres, A.K. Geim, Science 320 (2008) 1308.
[23] F. Schwierz, Nature Nanotechnology 5 (2010) 487–496.

[24] S. Stankovich, D.A. Dikin, G.H.B. Dommett, K.M. Kohlhaas, E.J. Zimney, E.A. Stach, R.D. Piner, S.T. Nguyen, R.S. Ruoff, Nature 442 (2006) 282–286.
[25] S. Bae, H. Kim, Y. Lee, X.F. Xu, J.S. Park, Y. Zheng, J. Balakrishnan, T. Lei, H.R. Kim, Y.I. Song, Y.J. Kim, K.S. Kim, B. Ozyilmaz, J.H. Ahn, B.H. Hong, S. Iijima, Nature Nanotechnology 5 (2010) 574–578.
[26] X. Wang, L. Zhi, K. Müllen, Nano Letters 8 (2008) 323–327.
[27] J. Wu, M. Agrawal, H.A. Becerril, Z. Bao, Z. Liu, Y. Chen, P. Peumans, ACS nano 4 (2009) 43–48.
[28] F. Bonaccorso, Z. Sun, T. Hasan, A.C. Ferrari, Nature Photonics 4 (2010) 611–622.
[29] F. Schedin, A.K. Geim, S.V. Morozov, E.W. Hill, P. Blake, M.I. Katsnelson, K.S. Novoselov, Nature Materials 6 (2007) 652–655.
[30] S. Park, R.S. Ruoff, Nature Nanotechnology 4 (2009) 217–224.
[31] D.A. Dikin, S. Stankovich, E.J. Zimney, R.D. Piner, G.H.B. Dommett, G. Evmenenko, S.T. Nguyen, R.S. Ruoff, Nature 448 (2007) 457–460.
[32] Y. Hernandez, V. Nicolosi, M. Lotya, F.M. Blighe, Z. Sun, S. De, I. McGovern, B. Holland, M. Byrne, Y.K. Gun'Ko, Nature Nanotechnology 3 (2008) 563–568.
[33] N. Behabtu, J.R. Lomeda, M.J. Green, A.L. Higginbotham, A. Sinitskii, D.V. Kosynkin, D. Tsentalovich, A.N.G. Parra-Vasquez, J. Schmidt, E. Kesselman, Nature Nanotechnology 5 (2010) 406–411.
[34] Y.Q. Sun, Q.O. Wu, G.Q. Shi, Energy & Environmental Science 4 (2011) 1113–1132.
[35] M.J. Allen, V.C. Tung, R.B. Kaner, Chemical Reviews 110 (2010) 132–145.
[36] C. Berger, Z. Song, X. Li, X. Wu, N. Brown, C. Naud, D. Mayou, T. Li, J. Hass, A.N. Marchenkov, Science 312 (2006) 1191–1196.
[37] K.S. Kim, Y. Zhao, H. Jang, S.Y. Lee, J.M. Kim, J.H. Ahn, P. Kim, J.Y. Choi, B.H. Hong, Nature 457 (2009) 706–710.
[38] A.K. Geim, Science 324 (2009) 1530–1534.
[39] D. Chen, L.H. Tang, J.H. Li, Chemical Society Reviews 39 (2010) 3157–3180.
[40] D.C. Wei, Y.Q. Liu, Y. Wang, H.L. Zhang, L.P. Huang, G. Yu, Nano Letters 9 (2009) 1752–1758.
[41] M. Segal, Nature Nanotechnology 4 (2009) 611–613.
[42] Z.S. Wu, D.W. Wang, W. Ren, J. Zhao, G. Zhou, F. Li, H.M. Cheng, Advanced Functional Materials 20 (2010) 3595–3602.
[43] H.C. Schniepp, J.L. Li, M.J. McAllister, H. Sai, M. Herrera-Alonso, D.H. Adamson, R.K. Prud'homme, R. Car, D.A. Saville, I.A. Aksay, Journal of Physical Chemistry B 110 (2006) 8535–8539.
[44] Y.W. Zhu, S. Murali, M.D. Stoller, K.J. Ganesh, W.W. Cai, P.J. Ferreira, A. Pirkle, R.M. Wallace, K.A. Cychosz, M. Thommes, D. Su, E.A. Stach, R.S. Ruoff, Science 332 (2011) 1537–1541.
[45] A.G. Pandolfo, A.F. Hollenkamp, Journal of Power Sources 157 (2006) 11–27.
[46] H. Wang, Q. Hao, X. Yang, L. Lu, X. Wang, Electrochemistry Communications 11 (2009) 1158–1161.
[47] Y. Li, L. Tang, J. Li, Electrochemistry Communications 11 (2009) 846–849.
[48] Y. Chen, X. Zhang, D. Zhang, P. Yu, Y. Ma, Carbon 49 (2011) 573–580.
[49] L. Tang, Y. Wang, Y. Li, H. Feng, J. Lu, J. Li, Advanced Functional Materials 19 (2009) 2782–2789.
[50] W. Li, C. Liang, W. Zhou, J. Qiu, Z. Zhou, G. Sun, Q. Xin, Journal of Physical Chemistry B 107 (2003) 6292–6299.
[51] K. Gong, F. Du, Z. Xia, M. Durstock, L. Dai, Science 323 (2009) 760–764.
[52] E.K. Choi, I.Y. Jeon, S.Y. Bae, H.J. Lee, H.S. Shin, L. Dai, J.B. Baek, Chemical Communications 46 (2010) 6320–6322.
[53] J. Hernandez, J. Solla-Gullon, E. Herrero, Journal of Electroanalytical Chemistry 574 (2004) 185–196.
[54] J. Luo, M.M. Maye, V. Petkov, N.N. Kariuki, L. Wang, P. Njoki, D. Mott, Y. Lin, C.J. Zhong, Chemistry of Materials 17 (2005) 3086–3091.
[55] R. Kou, Y. Shao, D. Wang, M.H. Engelhard, J.H. Kwak, J. Wang, V.V. Viswanathan, C. Wang, Y. Lin, Y. Wang, Electrochemistry Communications 11 (2009) 954–957.
[56] L. Dong, R.R.S. Gari, Z. Li, M.M. Craig, S. Hou, Carbon 48 (2010) 781–787.
[57] H. Dai, Nature Materials 10 (2011) 780–786.
[58] S. Guo, S. Dong, E. Wang, ACS Nano 4 (2009) 547–555.
[59] L. Qu, Y. Liu, J.B. Baek, L. Dai, ACS nano 4 (2010) 1321–1326.
[60] S. Yang, X. Feng, X. Wang, K. Müllen, Angewandte Chemie International Edition 50 (2011) 5339–5343.
[61] S.M. Choi, M.H. Seo, H.J. Kim, W.B. Kim, Carbon 49 (2010) 904–909.
[62] E.J. Yoo, T. Okata, T. Akita, M. Kohyama, J. Nakamura, I. Honma, Nano Letters 9 (2009) 2255–2259.
[63] C.V. Rao, A.L.M. Reddy, Y. Ishikawa, P.M. Ajayan, Carbon 49 (2011) 931–936.
[64] P.B. Balbuena, D. Altomare, N. Vadlamani, S. Bingi, L.A. Agapito, M. Jorge, Journal of Physical Chemistry A 108 (2004) 6378–6384.
[65] T. Toda, H. Igarashi, H. Uchida, M. Watanabe, Journal of the Electrochemical Society 146 (1999) 3750–3756.
[66] S. Zhang, Y. Shao, H. Liao, J. Liu, I.A. Aksay, G. Yin, Y. Lin, Chemistry of Materials 23 (2011) 1079–1081.
[67] S. Zhang, Y. Shao, G. Yin, Y. Lin, Journal of Materials Chemistry 19 (2009) 7995–8001.
[68] N. Kristian, Y. Yan, X. Wang, Chemical Communications (2008) 353–355.
[69] S. Wang, X. Wang, Physical Chemistry Chemical Physics 13 (2011) 6883–6891.
[70] Y. Zhang, Y. Gu, S. Lin, J. Wei, Z. Wang, C. Wang, Y. Du, W. Ye, Electrochimica Acta 56 (2011) 8746–8751.
[71] I.Y. Jeon, D. Yu, S.Y. Bae, H.J. Choi, D.W. Chang, L. Dai, J.B. Baek, Chemistry of Materials 23 (2011) 3987–3992.
[72] D.H. Lee, W.J. Lee, S.O. Kim, Y.H. Kim, Physical Review Letters 106 (2011) 175502–175505.
[73] E. Frackowiak, J. Machnikowski, F. Béguin, Novel Carbonaceous Materials for Application in the Electrochemical Supercapacitors, New Carbon Based Materials for Electrochemical Energy Storage Systems: Batteries, Supercapacitors and Fuel Cells, 1st ed., Springer, Netherlands, Dordrecht, The Netherlands, 2006, pp. 5–20.
[74] P. Simon, Y. Gogotsi, Nature Materials 7 (2008) 845–854.
[75] R. Kötz, M. Carlen, Electrochimica Acta 45 (2000) 2483–2498.
[76] Y.R. Nian, H. Teng, Journal of the Electrochemical Society 149 (2002) A1008–A1014.
[77] E. Frackowiak, K. Metenier, V. Bertagna, F. Beguin, Applied Physics Letters 77 (2000) 2421–2423.
[78] V. Subramanian, H. Zhu, R. Vajtai, P. Ajayan, B. Wei, Journal of Physical Chemistry B 109 (2005) 20207–20214.
[79] A. Rudge, J. Davey, I. Raistrick, S. Gottesfeld, J.P. Ferraris, Journal of Power Sources 47 (1994) 89–107.
[80] A. Laforgue, P. Simon, C. Sarrazin, J.F. Fauvarque, Journal of Power Sources 80 (1999) 142–148.
[81] E. Frackowiak, F. Beguin, Carbon 39 (2001) 937–950.
[82] M.D. Stoller, S. Park, Y. Zhu, J. An, R.S. Ruoff, Nano Letters 8 (2008) 3498–3502.
[83] J. Xia, F. Chen, J. Li, N. Tao, Nature Nanotechnology 4 (2009) 505–509.
[84] J. Yan, T. Wei, B. Shao, F. Ma, Z. Fan, M. Zhang, C. Zheng, Y. Shang, W. Qian, F. Wei, Carbon 48 (2010) 1731–1737.
[85] G. Yu, L. Hu, M. Vosgueritchian, H. Wang, X. Xie, J.R. McDonough, X. Cui, Y. Cui, Z. Bao, Nano Letters 11 (2011) 2905–2911.
[86] P. Mini, A. Balakrishnan, S.V. Nair, K. Subramanian, Chemical Communications 47 (2011) 5753–5755.

[87] H. Wang, Q. Hao, X. Yang, L. Lu, X. Wang, Nanoscale 2 (2010) 2164–2170.
[88] J.J. Yoo, K. Balakrishnan, J. Huang, V. Meunier, B.G. Sumpter, A. Srivastava, M. Conway, A.L. Mohana Reddy, J. Yu, R. Vajtai, Nano Letters 11 (2011) 1423–1427.
[89] C. Liu, Z. Yu, D. Neff, A. Zhamu, B.Z. Jang, Nano Letters 10 (2010) 4863–4868.
[90] Q. Du, M. Zheng, L. Zhang, Y. Wang, J. Chen, L. Xue, W. Dai, G. Ji, J. Cao, Electrochimica Acta 55 (2010) 3897–3903.
[91] H.M. Jeong, J.W. Lee, W.H. Shin, Y.J. Choi, H.J. Shin, J.K. Kang, J.W. Choi, Nano Letters 11 (2011) 2472–2477.
[92] Z. Fan, J. Yan, L. Zhi, Q. Zhang, T. Wei, J. Feng, M. Zhang, W. Qian, F. Wei, Advanced Materials 22 (2010) 3723–3728.
[93] C.X. Guo, C.M. Li, Energy & Environmental Science 4 (2011) 4504–4507.
[94] F. Alvi, M.K. Ram, P.A. Basnayaka, E. Stefanakos, Y. Goswami, A. Kumar, Electrochimica Acta 56 (2011) 9406–9412.
[95] G. Yu, L. Hu, N. Liu, H. Wang, M. Vosgueritchian, Y. Yang, Y. Cui, Z. Bao, Nano Letters 11 (2011) 4438–4442.
[96] X. Xia, J. Tu, Y. Mai, R. Chen, X. Wang, C. Gu, X. Zhao, Chemistry A: European Journal 17 (2011) 10898–10905.
[97] Q. Qu, S. Yang, X. Feng, Advanced Materials 23 (2011) 5574–5580.
[98] W. Lv, D.M. Tang, Y.B. He, C.H. You, Z.Q. Shi, X.C. Chen, C.M. Chen, P.X. Hou, C. Liu, Q.H. Yang, ACS Nano 3 (2009) 3730–3736.
[99] Y. Xu, K. Sheng, C. Li, G. Shi, ACS nano 4 (2010) 4324–4330.
[100] G. Shi, L. Zhang, Journal of Physical Chemistry C 115 (2011) 17206–17212.
[101] X. Wang, X. Li, L. Zhang, Y. Yoon, P.K. Weber, H. Wang, J. Guo, H. Dai, Science 324 (2009) 768–771.
[102] Y. Wang, Y. Shao, D.W. Matson, J. Li, Y. Lin, ACS Nano 4 (2010) 1790–1798.
[103] Y. Qiu, X. Zhang, S. Yang, Physical Chemistry Chemical Physics 13 (2011) 12554–12558.
[104] D. Yu, L. Dai, Journal of Physical Chemistry Letters 1 (2009) 467–470.
[105] F. Du, D. Yu, L. Dai, S. Ganguli, V. Varshney, A. Roy, Chemistry of Materials 23 (2011) 4810–4816.
[106] A.F. Diaz, J.I. Castillo, J. Logan, W.Y. Lee, Journal of Electroanalytical Chemistry and Interfacial Electrochemistry 129 (1981) 115–132.
[107] D. Ofer, R.M. Crooks, M.S. Wrighton, Journal of the American Chemical Society 112 (1990) 7869–7879.
[108] M.L. Guo, J.H. Chen, J. Li, B. Tao, S.Z. Yao, Analytica Chimica Acta 532 (2005) 71–77.
[109] D.W. Wang, F. Li, J. Zhao, W. Ren, Z.G. Chen, J. Tan, Z.S. Wu, I. Gentle, G.Q. Lu, H.M. Cheng, ACS Nano 3 (2009) 1745–1752.
[110] K. Zhang, L.L. Zhang, X. Zhao, J. Wu, Chemistry of Materials 22 (2010) 1392–1401.
[111] W. Lu, A.G. Fadeev, B. Qi, E. Smela, B.R. Mattes, J. Ding, G.M. Spinks, J. Mazurkiewicz, D. Zhou, G.G. Wallace, Science 297 (2002) 983–987.
[112] A. Davies, B. Farrow, P. Audette, F. Hassan, Z. Chen, J.Y. Choi, A. Yu, Journal of Physical Chemistry C 115 (2011) 17612–17620.
[113] H.W. Wang, Z.A. Hu, Y.Q. Chang, Y.L. Chen, Z.Q. Lei, Z.Y. Zhang, Y.Y. Yang, Electrochimica Acta 55 (2010) 8974–8980.
[114] N. Nagarajan, M. Cheong, I. Zhitomirsky, Materials Chemistry and Physics 103 (2007) 47–53.
[115] J. Yan, Z. Fan, T. Wei, W. Qian, M. Zhang, F. Wei, Carbon 48 (2010) 3825–3833.
[116] S. Chen, J. Zhu, X. Wu, Q. Han, X. Wang, ACS Nano 4 (2010) 2822–2830.
[117] T. Lu, Y. Zhang, H. Li, L. Pan, Y. Li, Z. Sun, Electrochimica Acta 55 (2010) 4170–4173.
[118] F. Li, J. Song, H. Yang, S. Gan, Q. Zhang, D. Han, A. Ivaska, L. Niu, Nanotechnology 20 (2009) 455602.
[119] Y.L. Chen, Z.A. Hu, Y.Q. Chang, H.W. Wang, Z.Y. Zhang, Y.Y. Yang, H.Y. Wu, Journal of Physical Chemistry C 115 (2011) 2563–2571.
[120] J. Zheng, P. Cygan, T. Jow, Journal of the Electrochemical Society 142 (1995) 2699–2703.
[121] J.T. Zhang, J.W. Jiang, H.L. Li, X.S. Zhao, Energy & Environmental Science 4 (2011) 4009–4015.
[122] S. Chen, J.W. Zhu, X. Wang, Journal of Physical Chemistry C 114 (2010) 11829–11834.
[123] J. Yan, T. Wei, W. Qiao, B. Shao, Q. Zhao, L. Zhang, Z. Fan, Electrochimica Acta 55 (2010) 6973–6978.
[124] H.W. Wang, Z.A. Hu, Y.Q. Chang, Y.L. Chen, H.Y. Wu, Z.Y. Zhang, Y.Y. Yang, Journal of Materials Chemistry 21 (2011) 10504–10511.

Hyun-Jung Choi is a PhD candidate in the Prof. Jong-Beom Baek group. She received her M.S. degree (2008) in Interdisciplinary School of Green Energy from Ulsan National Institute of Science and Technology (UNIST), Korea. Her thesis is focused on carbon nanotube/metal nanoparticle composite. Her current research work is chemically functionalized graphene derivatives for use in electrochemical energy conversion and storage.

Sun-Min Jung is under combined master's-doctoral program in the Prof. Jong-Beom Baek group in Interdisciplinary School of Green Energy from Ulsan National Institute of Science and Technology (UNIST), Korea. She received her B.S. degree in Chemical Engineering from Chungbuk National University in 2011. Her current research work is heteroatom-doped graphene materials *via* wet-chemical synthesis and their applications for electrochemical energy conversion and storage.

Jeong-Min Seo is under combined master's-doctoral program in the Prof. Jong-Beom Baek group in Interdisciplinary School of Green Energy from Ulsan National Institute of Science and Technology (UNIST), Korea. She received her B.S. degree in Fine Chemical Engineering and Applied Chemistry from Chungnam National University in 2011. Her current research work is chemical functionalization of graphene via Diels-Alder reaction.

Dong Wook Chang is an assistant professor and department chair of Chemical Systematic Engineering at Catholic University of Daegu, South Korea. He obtained his B.S. and M.S. degrees from Fiber and Polymer Engineering at Seoul National University, South Korea. In 2003, he joined Prof. Liming Dai's group and obtained Ph. D. from Materials Engineering at the University of Dayton in 2007. Prior to joining current position, he worked for two years as a research assistant professor of the Interdisciplinary School of Green Energy at Ulsan National University of Science and Technology (UNIST). His research interest is the synthesis of conjugated molecules and functionalization of carbon nanomaterials for renewable energy applications.

Liming Dai is the Kent Hale Smith Professor in the Department of Macromolecular Science and Engineering at Case Western Reserve University (CWRU). He is also director of the Center of Advanced Science and Engineering for Carbon (CASE4Carbon). Prior to joining the CWRU, he was an associate professor of polymer engineering at the University of Akron and the Wright Brothers Institute Endowed Chair Professor of Nanomaterials at the University of Dayton. Dr. Dai's expertise lies across the synthesis, chemical modification and device fabrication of conjugated polymers and carbon nanomaterials for energy-related and biomedical applications.

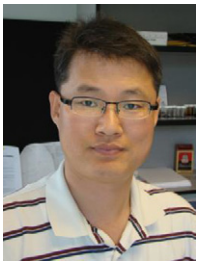

Jong-Beom Baek is an associate professor of the Interdisciplinary School of Green Energy and a director of Low-Dimensional Carbon Materials Center (LCMC) at Ulsan National Institute of Science and Technology (UNIST, Korea). He obtained a PhD in Polymer Science from the University of Akron (USA). Prior to joining the UNIST, he was an associate professor of Industrial Chemistry at Chungbuk National University (Korea) and a research chemist at the Wright–Patterson Air Force Research Laboratory (AFRL). Dr. Baek's current research interest is the defect-selective functionalization of carbon nanomaterials for application-specific purposes.